Available online at www.sciencedirect.com

SciVerse ScienceDirect

Ceramics International 38 (2012) 6753–6767

CERAMICS INTERNATIONAL

www.elsevier.com/locate/ceramint

A kinetic study on the electrophoretic deposition of hydroxyapatite–titania nanocomposite based on a statistical approach

Hamidreza Farnoush[a], Jamshid Aghazadeh Mohandesi[a,*], Davoud Haghshenas Fatmehsari[a], Fathollah Moztarzadeh[b]

[a]*Department of Mining and Metallurgical Engineering, Amirkabir University of Technology, P.O. Box 15875-4413, Tehran, Iran*
[b]*Biomedical Engineering Department, Amirkabir University of Technology, P.O. Box 15875-4413, Tehran, Iran*

Received 11 April 2012; received in revised form 22 May 2012; accepted 22 May 2012
Available online 6 June 2012

Abstract

In the present study, the electrophoretic deposition (EPD) process of hydroxyapatite–titania nanocomposite was kinetically described by the use of response surface methodology (RSM). The electrostatic interaction between particles in ethanol based suspensions was determined by Zeta potential and particle size analyses. After successful electrophoretic deposition from hydroxyapatite–titania suspensions with 0, 10 and 20 wt% of titania nanoparticles, it was shown that Baldisserri model can well reproduce the experimental data among the other semi-empirical kinetic equations. The as-deposited hydroxyapatite–titania nanocomposites were characterized employing SEM, AFM, XRD, and FT-IR analyses. Then, the effects of deposition voltage, deposition time and wt% TiO_2 on the kinetic of EPD at two time intervals (10–60 s and 60–300 s) were identified and quantified via RSM based on a central composite design (CCD). According to the results obtained from the statistical analysis, it was found that the deposition rate decreases by an increase in wt% TiO_2 and time. Also, a transition in deposition mechanism from linear to parabolic mode was observed and two second order polynomial equations were fitted to the response (deposit weight) at each time intervals.

Keywords: B. Nanocomposites; D. Apatite; D. TiO_2; Electrophoretic deposition

1. Introduction

Hydroxyapatite (HA, $Ca_{10}(PO_4)_6(OH)_2$), the main constituent of the bone and teeth, is known as a biocompatible ceramic material with high osseoconductivity [1]. Many efforts have been focused on developing HA coatings on tough metallic substrates (composite and/or hybrid systems) to compensate its intensive brittle nature [2–5]. In this way, both the mechanical characteristics of metallic substrates and the biological performances of HA ceramics are achieved simultaneously [1]. Among different methods employed for the fabrication of HA coatings on a metallic substrate, such as plasma spray [6,7], sol–gel [8,9], biomimetic [10,11] and ion implantation [12], electrophoretic deposition (EPD) [13–15] is an effective technique for the fabrication of dense and uniform HA layers on a substrate even with complex geometries. This technique has the advantages of high production rate and low investment cost [16].

The difficulties in EPD of HA particles, including low bonding strength between HA and metallic substrate [17], thermal instability of HA [18], firing shrinkage of HA coating [18], and thermal expansion coefficient mismatch between HA and the substrate [19], lead to insufficient densification of HA coatings, crack formation in HA coating–metallic substrate interface and/or HA decomposition. An approach to cope with above mentioned problems is the use of titanium oxide (TiO_2) due to its superior corrosion behavior (acting as a chemical barrier against the release metal ions [19,20]), positive effect on the interfacial bond strength [17,20] and constructive role in the overall performance of HA coating systems [20,21]. Additionally, the presence of TiO_2 in HA coatings hinders the crack propagation and improves the thermal expansion coefficient of HA [20–22].

---

*Corresponding author. Tel.: 98 21 64542949; fax: 98 21 64542941.
E-mail addresses: farnoush@aut.ac.ir (H. Farnoush), jamshidaghazadeh@gmail.com (J. Aghazadeh Mohandesi).

0272-8842/$36.00 © 2012 Elsevier Ltd and Techna Group S.r.l. All rights reserved.
http://dx.doi.org/10.1016/j.ceramint.2012.05.070

In an EPD process, the colloidal particles in a stable suspension are deposited onto an electrode under an applied electrical field [16]. The stability of the suspensions and the quality of final product are significantly influenced by the kinetic behavior of suspended particles in the media [23]. The rate of EPD process is, also, a function of electrical field and particle size (especially in a suspension of particles with different sizes [24]).

The simplest model describing the kinetics of EPD is known as the Hamaker model; a linear correlation between the deposition yield (W) and, suspension concentration (C_s), electrophoretic mobility (μ), applied electric field strength (E), deposition area (A) and deposition time (t). In a cell with planar geometry, Hamaker equation can be written as [25]

$$\mathrm{W(t)} = \mathrm{C}_s\mu\mathrm{AEt} \tag{1}$$

It should be mentioned that Hamaker model is only valid at initial times of deposition process [23] because the decrease in the concentration of suspended particles by EPD proceeding has been disregarded.

Another model, which considers the variation in suspended particles concentration, was proposed by Zhang [26]:

$$W(t) = W_0(1-e^{-kt}) \quad \text{with } k = \frac{fA\varepsilon_0\varepsilon_r\zeta E}{4\pi V\eta} \tag{2}$$

where W_0 is the initial concentration of suspended particles; ($\varepsilon_0\varepsilon_r$), ζ, η and V are the permittivity, Zeta potential, viscosity and volume of the suspension medium, respectively. Also, f is a correction factor. However, the shielding effect of growing layer is ignored by this model.

Recently, Baldisserri et al. [27] have developed a mathematical correlation between some characteristics of TiO_2 deposits (such as thickness, density and resistivity) and the electrical current flow in EPD process for an ethanol based colloidal suspension as

$$W(t) = \frac{2Akj_0}{\alpha}(\sqrt{1+\alpha t}-1) \quad \text{with} \quad \alpha = \frac{2j_0^2k}{E}\left(\frac{\rho_D}{d_D}\right) \tag{3}$$

where A is the working electrode area, k is the ratio between deposited mass and passed charge, j_0 is the initial current density, V is the deposition voltage, ρ_D is the resistivity of deposit, and d_D the density of deposit. This correlation considers both the concentration variation of suspended particles and shielding effect of growing layer.

A literature review shows that the appropriate choice of the value of the parameters, such as suspended particles' concentration [28,29], pH of suspension [28,30], electrode separation [28,31], deposition voltage [28,32], and deposition time [28,32], is critical for a successful implementation of EPD process. Design of Experiments (DOE) is a powerful and reliable strategy for the correct identification of the pertinent factors in many types of systems and processes [33–35]. The application of DOE strategy in an EPD process has been limited to factorial design of experiments [31,36] and Taguchi method [37,38].

It has been shown that full factorial DOE as well as fractional factorial DOE gives the most complete information regarding interaction between parameters but the number of experiments becomes excessive in the former [34]. Fractional factorial designs (FFD), such as central composite design (CCD), can give information regarding parameter interactions with the use of less experimentation. On the other hand, response surface methodology (RSM) is well known as a much more suitable experimental approach than Taguchi method which is able to simultaneously consider several factors at different levels, and give a second order polynomial model for the relationship between the various factors and the response [39].

The aim of the present study is to elucidate the kinetics of electrophoretic deposition of HA–TiO_2 nanocomposite. In this regard, Zeta potential measurement and particle size analysis are employed to examine the electrostatic interaction between the particles in ethanol based suspensions. The effect of titania nanoparticles in as-deposited hydroxyapatite–titania nanocomposites were characterized by SEM, AFM, XRD, and FT-IR analyses. Then, the measured deposit weights are compared with the predictions obtained by Hamaker, Zhang and Baldisserri models. Finally, the effects of deposition voltage, deposition time and TiO_2 wt% on EPD kinetics are evaluated by the use of response surface methodology. A central composite design is chosen as the design matrix since it allows reliable evaluation of first order interaction between parameters and provides a second order polynomial model.

2. Experimental details

2.1. Materials

Hydroxyapatite (Merck, USA) and TiO_2 (Degussa, Germany) powders were used as the coating materials. FE-SEM micrographs of as-received particles are presented in Fig. 1. The mean particle size (d_{50}) of hydroxyapatite and TiO_2 are ~250 and 21 nm, respectively. The substrate is a 3-mm-thick mill-annealed Ti–6Al–4V plate with the chemical composition (wt. %) as follows: Al=6.28, V=4.90, Fe=0.29, Nb=0.05, Mn=0.03, Cr=0.02, Si=0.05, Sn<0.05, Mo<0.03, Cu<0.02, Zr<0.01, and Ti. Three suspensions were individually prepared by adding 1 g of HA (H), HA–10 wt% TiO_2 (H10T), and HA–20 wt% TiO_2 (H20T) powder

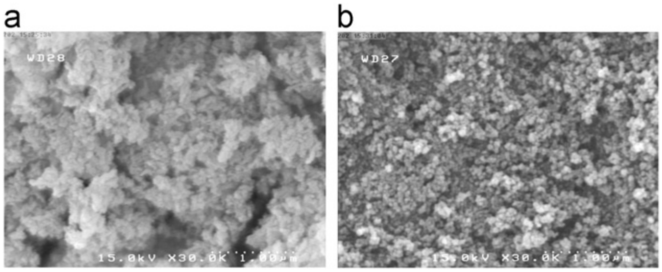

Fig. 1. FE-SEM micrographs of as-received (a) HA and (b) TiO_2 powders.

mixtures into 50 mL of absolute ethanol (Merck, USA). The addition of 1 g/L iodine (dispersant) to ethanol resulted in positively charged particles.

2.2. Methods

The prepared suspensions were dispersed by a 50 kHz ultrasonic bath for 60 min, and then were immediately used for EPD without further aging. Zeta potential and particle size distribution of the powders in suspensions were analyzed by Zetasizer (Malvern ZEN 3600). All measurements were carried out with slurries containing a 0.4 g/L solid loading. Ti–6Al–4V substrate (as the working electrode) and 316 L stainless steel (as the counter electrode) were immersed in the suspension with a fixed distance of 10 mm. Prior to deposition, Ti6Al4V substrates were ground by 400–1200 grit SiC papers, then washed out with detergent and degreased with acetone, and finally passivated by a HF (100 mL/L)–HNO_3 (300 mL/L) solution. One side of the cathode was masked by a non-conducting tape. Surface area of the cathode was 1 cm^2. EPD process was conducted within 10–300 s under constant voltages of 20, 40, and 60 V. During deposition, cell current was recorded by chronoamperometry. After deposition, the green coatings were dried in air for 24 h at room temperature and then weighted and accordingly the relationship between the passed charge in the deposition cell and the deposited mass was determined. The micro-structural characterization and elemental composition of as-deposited samples were analyzed by using scanning electron microscope (SEM, Philips XL 30) equipped with an Energy Dispersive Spectrometer (EDS). The structure of the coatings was evaluated by Fourier transform infrared (FTIR, Nicolet Nexus 670) spectroscopy in the wave number range of 4000–400 cm^{-1}. Phase composition of the coated surface was analyzed by X-ray diffraction (XRD, Philips PW 1480), in the $2\theta = 20$–100° range at a step size of 0.02° and a count time of 0.6 s. Surface roughness and topography were characterized by Scanning Probe Microscopy (SPM, DME DS-95–50E).

Table 1
Central composite design arrangement and response (weight of deposition as mean).

Number	Factors (10–60 s)			Response (10–60 s)	Factors (60–300 s)			Response (60–300 s)
	V (V)	time (s)	%TiO_2	W (g)	V (V)	time (s)	%TiO_2	W (g)
1	20	10	0	0.00116	20	60	0	0.0059
2	60	10	0	0.00249	60	60	0	0.0103
3	20	60	0	0.00590	20	300	0	0.0173
4	60	60	0	0.01030	60	300	0	0.0259
5	20	10	20	0.00139	20	60	20	0.0054
6	60	10	20	0.00216	60	60	20	0.0093
7	20	60	20	0.00540	20	300	20	0.0136
8	60	60	20	0.00930	60	300	20	0.0180
9	20	35	10	0.00400	20	180	10	0.0095
10	60	35	10	0.00749	60	180	10	0.0170
11	40	10	10	0.00160	40	60	10	0.0097
12	40	60	10	0.00900	40	300	10	0.0223
13	40	35	0	0.00550	40	180	0	0.0174
14	40	35	20	0.00473	40	180	20	0.0157
15	40	35	10	0.00570	40	180	10	0.0162
16	40	35	10	0.00580	40	180	10	0.0162
17	40	35	10	0.00550	40	180	10	0.0169

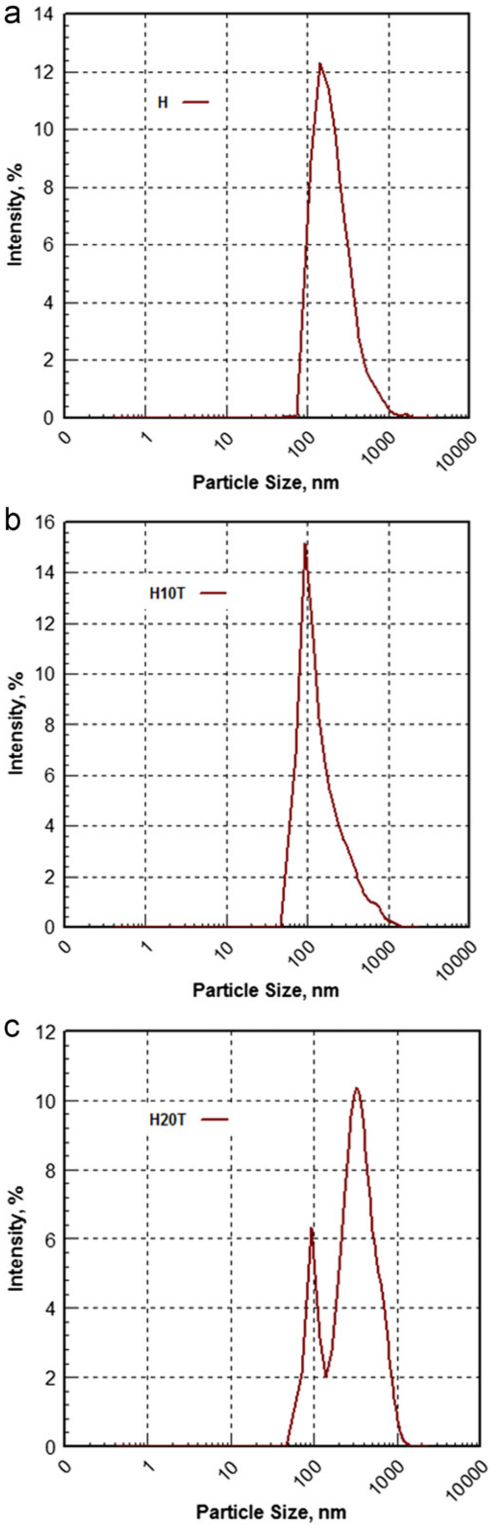

Fig. 2. Paticle size distribution in (a) H, (b) H10T, and (c) H20T samples.

Table 2
Measurements of particle size and Zeta potential for H, H10T, and H20T samples.

Sample	Mean particle size (nm)	Particle size distribution width (nm)	Zeta potential (mV)	Mobility (cm/Vs)	Cunductivity (mS/cm)
H	230.4	170.2	27 ± 0.9	1.44	0.021
H10T	172.6	148.5	21 ± 1.2	1.12	0.018
H20T	Peak 1: 98.43	20.34	16 ± 1.1	0.856	0.017
	Peak 2: 392.4	191.2			

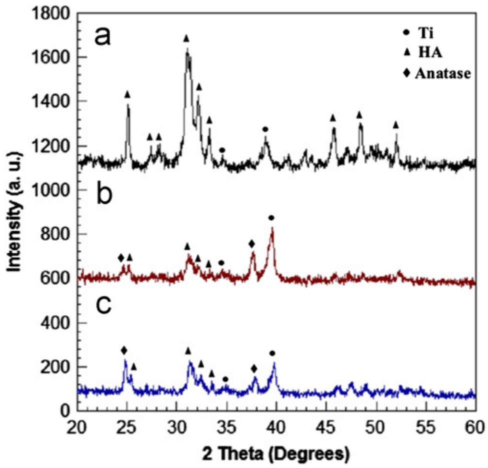

Fig. 3. XRD patterns of the as-deposited (a) H, (b) H10T and (c) H20T samples at 40 V after 90 s.

2.3. Experimental design for RSM

Response surface methodology (RSM) was employed to investigate the effect of deposition voltage (V), deposition time (time), and weight percentage of TiO_2 in suspension (%TiO_2) on deposition weight of H, H10T, and H20T specimens at two time intervals (10–60 s and 60–300 s). For each time interval, a central composite design (CCD) was adopted to study three factors at three levels. Seventeen experimental runs consisting of 6 star points (star distance is 0) and 3 center points were generated with 3 factors and 3 levels by the principle of RSM using MINITAB Release 15. The CCD design matrix which includes the levels employed for the different factors is presented in Table 1. The quadratic polynomial regression model, as follows, was chosen for predicting the responses variable in terms of the two independent variables chosen for the study [39]:

$$Y = b_0 + \sum_{i=1}^{3} b_i X_i + \sum_{i=1}^{3} b_{ii} X_i^2 + \sum_{i=1}^{2} \sum_{j=i+1}^{3} b_{ij} X_i X_j \qquad (4)$$

In this equation Y is the response variable b_0, b_i, b_{ii}, and b_{ij} are constant coefficients of intercept, linear, quadratic and interaction terms, respectively, and X_i and X_j represent the three independent variables (V, time, and %TiO_2). The experiments were carried with two replicates and conducted in a randomized order to avoid systematic bias.

The statistical significance of the full quadratic models predicted was evaluated by the analysis of variance (ANOVA). The significance and the magnitude of the effects were estimated for each variable and all their

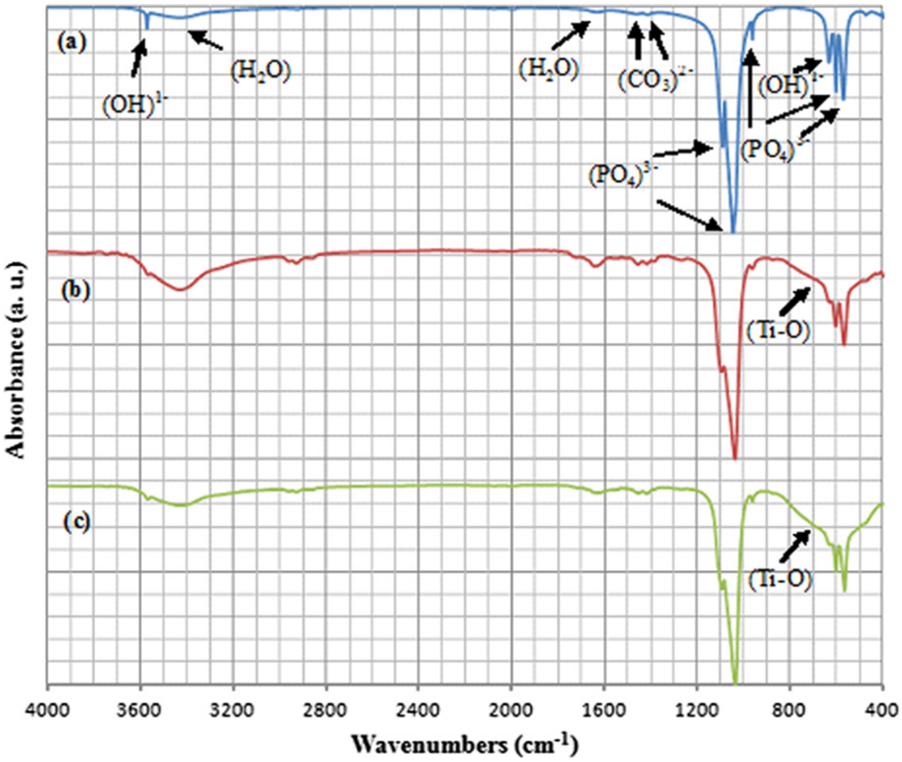

Fig. 4. The FTIR spectra of the as-deposited (a) H, (b) H10T and (c) H20T samples.

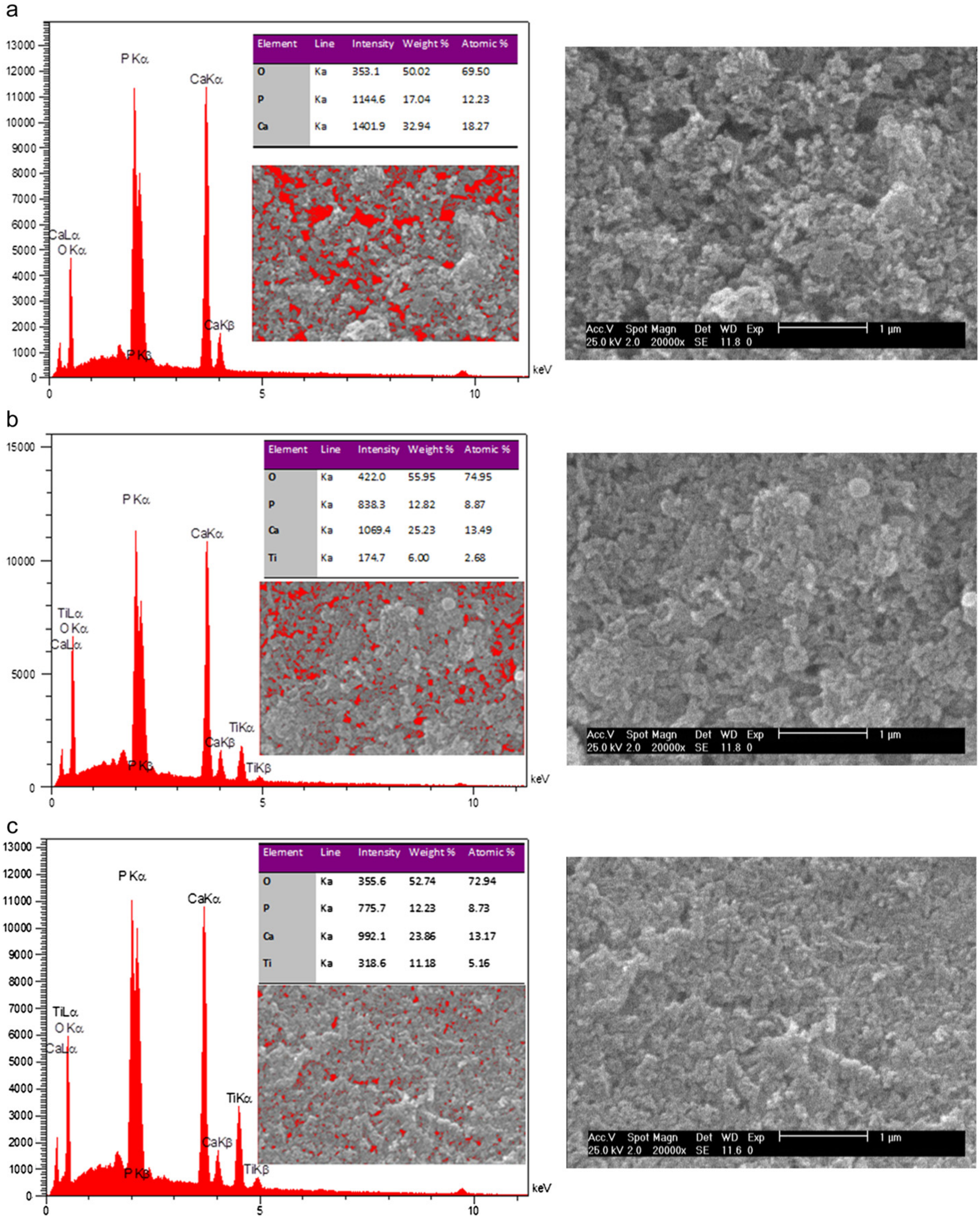

(a)

Element	Line	Intensity	Weight %	Atomic %
O	Ka	353.1	50.02	69.50
P	Ka	1144.6	17.04	12.23
Ca	Ka	1401.9	32.94	18.27

(b)

Element	Line	Intensity	Weight %	Atomic %
O	Ka	422.0	55.95	74.95
P	Ka	838.3	12.82	8.87
Ca	Ka	1069.4	25.23	13.49
Ti	Ka	174.7	6.00	2.68

(c)

Element	Line	Intensity	Weight %	Atomic %
O	Ka	355.6	52.74	72.94
P	Ka	775.7	12.23	8.73
Ca	Ka	992.1	23.86	13.17
Ti	Ka	318.6	11.18	5.16

Fig. 5. SEM micrographs, EDS spectra and the porosity of the as-deposited samples at 40 V after 60 s; (a) H, (b) H10T, and (c) H20T.

possible linear and quadratic interactions were also determined. Unless otherwise stated, the significance level employed in the analysis was 5% (p-value$=0.05$). All the analysis was carried out using MINITAB Release 15.

3. Results and discussion

3.1. Characterization of HA–TiO$_2$ suspensions and coatings

The stability/mobility of HA-based particulate suspensions influences the deposition rate of HA–TiO$_2$ coatings. Generally, suspension stability depends on the size of suspended particles [40], zeta potential and pH of the suspension [41], and the additives [42].

Fig. 2 illustrates particle size distribution corresponding to H, H10T and H20T samples. Two distinctive peaks, around 98 nm and 392 nm, in the curve belonging to H20T (Fig. 2c) are attributed to TiO$_2$ and HA particles, respectively. The appearance of one individual peak in Fig. 2a and b, contrary to Fig. 2c, is due to the low amount of TiO$_2$ in H and H10T samples.

In Table 2 the values of particle size, Zeta potential, mobility, and electrical conductivity, are listed for different suspensions. These results reveal that an increase in the amount of TiO$_2$ in HA–TiO$_2$ suspension leads to a decrease in Zeta potential. It is worthy of note that an increase in surface area of the suspended particles results in lower Zeta potential value due to higher electrolyte concentration [43,44]. Since the value of Zeta potential is the lowest for H20T sample, the coarsest HA aggregations are formed in this case (Fig. 2c). According to the results presented in Table 2, conductivity of the samples decreases by increasing TiO$_2$ in the suspension. Also, the electrophoretic motion of particles towards an oppositely charged electrode is driven by the determining potential ions adhered onto the particles' surface [24]. Thus, by increasing TiO$_2$ nanoparticles, only very few ionic charges are available and the driving force for particles motion is insufficient.

Fig. 3 illustrates X-ray patterns of as-deposited H, H10T, and H20T samples at 40 V after 90 s. In all spectra, the peaks that appeared at $2\theta=25.8°$, $28.7°$, $31°$, $32.1°$, $33.3°$, $45.7°$, $48.3°$ and $52°$ corresponded to (002), (210), (211), (112), (222) and (321) planes of hydroxyapatite crystal, respectively [45]. Furthermore, the characteristics peaks of TiO$_2$ (anatase) at $2\theta=25.3°$ and $37.4°$ are apparently distinguishable in H10T and H20T samples which are assigned to (101) and (004) planes, respectively [46].

FT-IR spectra of as-deposited samples are also shown in Fig. 4. The wave numbers of 570, 602, 1047, and 1090 cm^{-1} are related to PO$_4^{3-}$ functional groups which are present in all samples. The water associated with HA appears at 1630 and 3423 cm^{-1} and OH^{-} stretching vibration is observed at 632 and 3572 cm^{-1}. The blunt and smooth peaks, at 1470

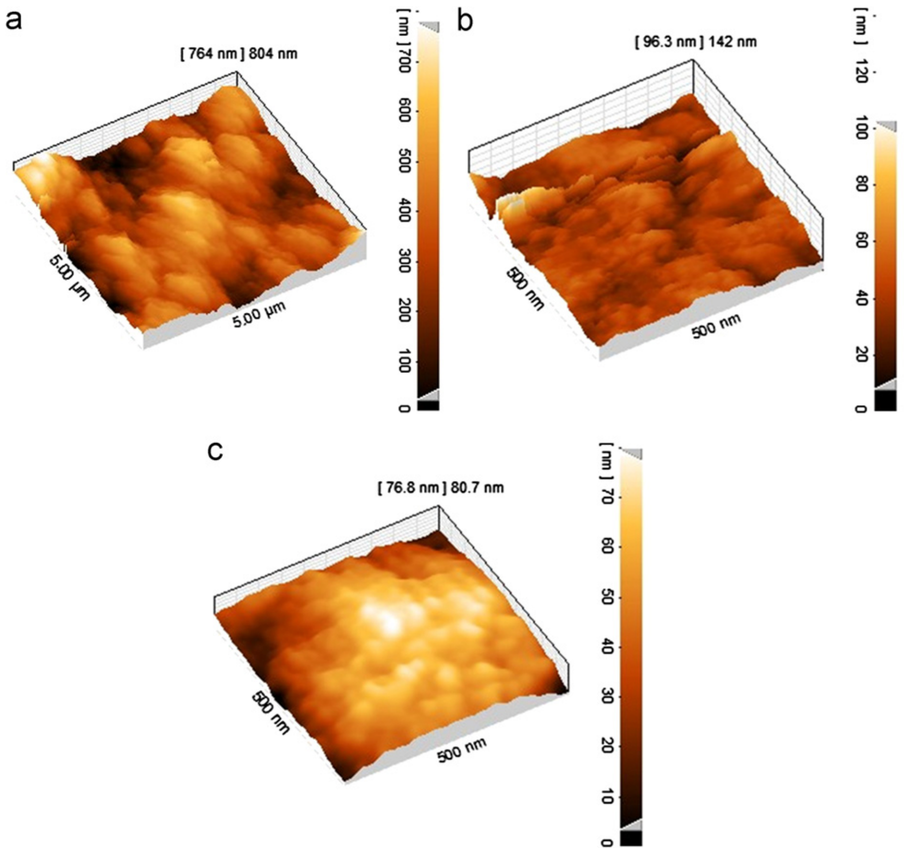

Fig. 6. AFM images of as-deposited (a) H, (b) H10T, and (c) H20T samples at 40 V after 60 s.

and 1420 cm^{-1}, are attributed to CO_3^{2-} ions which might be the result of the absorption of atmospheric CO_2 on the surface of HA particles [47]. However, these peaks are very weak which implies a very low carbonate content of the sample. The absorption peak at 700 cm^{1-} is the characteristic vibration peak of Ti–O bond confirming the presence of TiO_2 in H10T and H20T samples [48].

According to the SEM images presented in Fig. 5, the pores in H sample are larger than those in H20T. Also, the porosities of as-deposited H, H10T, and H20T samples, estimated by SEM image processing via ImageJ 1.45s software, are 12.4%, 8.5%, and 3.6%, respectively. This reveals that porosity effectively depends on TiO_2 content of the samples. From the EDS spectra of Ca, P, Ti and O in Fig. 5, it can be

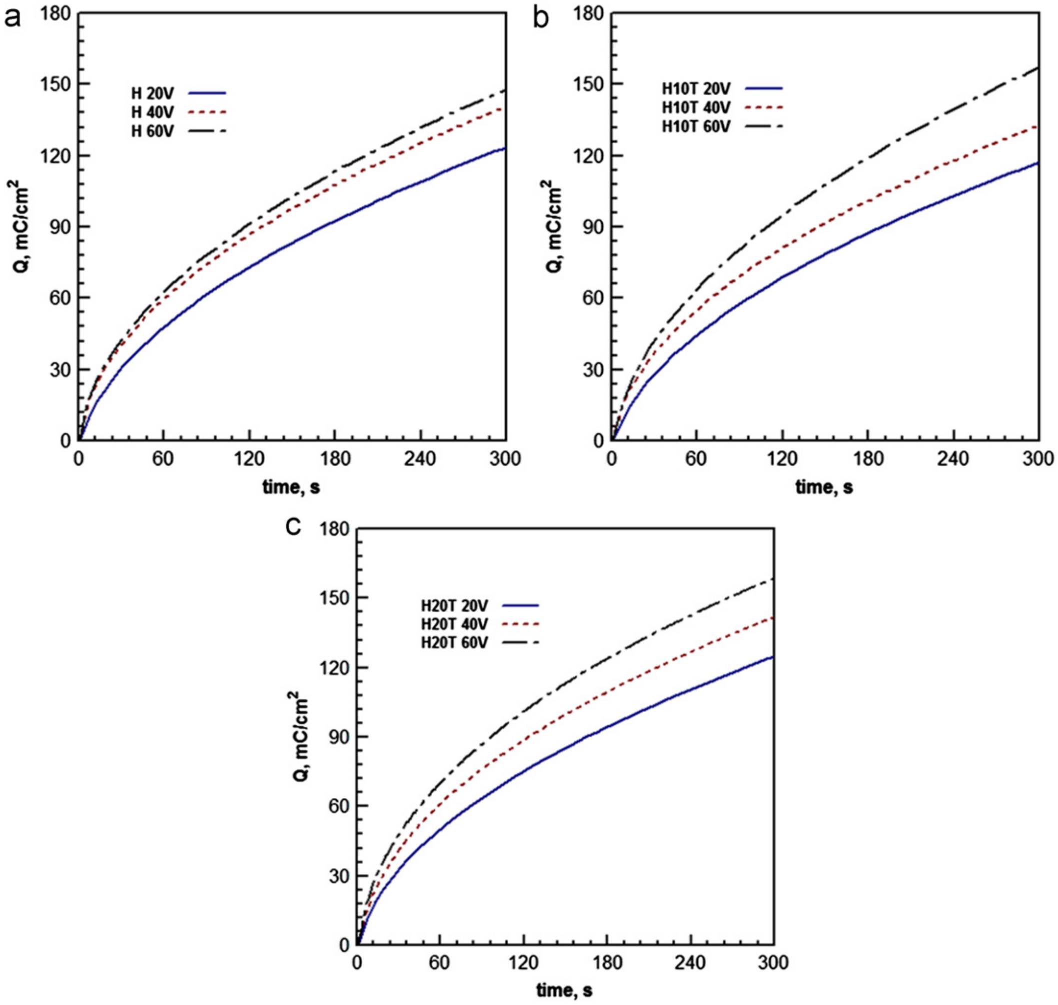

Fig. 7. Passed charge-deposition time curves of (a) H, (b) H10T, and (c) H20T samples deposited at different electric fields.

Table 3
Comparison of different kinetic models applied for EPD of HA–TiO_2 suspensions.

Sample	Voltage (V)	Baldisserri [27]				Zhang [26]		Hamaker [25]	
		α (s^{-1})	K_1 (mg/mc)	j_0 (mA/cm^2)	R^2	$k\times10^{-4}$ (s^{-1})	R^2	$k\times10^{-4}$ (s^{-1})	R^2
H	20	0.702	0.1340	3.15	0.9640	1.29	0.9321	6.33	0.9140
	40	2.37	0.1538	6.74	0.9910	1.79	0.8783	8.73	0.8445
	60	7.16	0.1850	11.6	0.9752	2.17	0.7552	10.5	0.6896
H10T	20	0.359	0.1260	2.24	0.9620	1.15	0.8739	5.66	0.8441
	40	2.59	0.1631	6.34	0.9888	1.71	0.8603	8.36	0.8233
	60	3.77	0.1483	8.95	0.9954	1.81	0.7608	8.83	0.6998
H20T	20	0.207	0.1046	1.88	0.9941	1.02	0.8669	5.01	0.8353
	40	1.02	0.1076	4.43	0.9719	1.19	0.6547	5.83	0.5749
	60	1.13	0.1110	5.23	0.9543	1.37	0.5835	6.73	0.4876

indicated that the composite coating contains 0, 9.01, and 18.68 wt% TiO_2 for H, H10T and H20T samples, respectively. Based on the AFM analysis corresponding to these three samples (Fig. 6), the average roughness height is 764 (H sample), 96.3 (H10T sample), and 76.8 (H20T sample) in nm. The higher porosity of H compared to H10T and H20T indicates the important role of titania particles in lowering surface roughness and densifying membrane.

3.2. Kinetics of deposition

Fig. 7 depicts the charge passed during EPD process versus time under different conditions. As can be observed, the passed charge (Q) variation with time shows a descending trend for all experimental conditions (Fig. 7a, b and c). However, due to the formation of an insulating layer composed of differently charged ceramic particles [49], dQ/dt approaches to a fixed value after a given time. Also, an increase in the deposition voltage leads to an increase in the passed charge during process which is due to a higher motion of the suspended particles. However, the slight difference between passed charges at 40 and 60 V can be ascribed to the change in EPD mechanisms from deposition controlling mode to diffusion controlling mode [50].

Kinetic modeling of the experimental data by the use of Hamaker (Eq. (1)), Zhang (Eq. (2)) and Baldisserri (Eq. (3)) models has been carried out and, the results of mathematical analyses are summarized in Table 3 for different samples (H, H10T and H20T). Values of R^2 indicate that Baldisserri model can well reproduce the experimental data which can be attributed to the fact that this model considers the insulating effect of growing layer [27]. It is worthy of note that EPD is a two-step process, electrophoresis and deposit formation [32]. Although electrophoretic motion of the suspended particles leads to the accumulation of particles at electrode surface, it does not necessarily result in the formation of deposit. Both Hamaker and Zhang assumed that all particles would be deposited at an infinite time [23]. However, by increasing the resistivity of deposit due to the formation of an insulating layer after initial times, the deposition rate drops.

Fig. 8 illustrates that the deposition yields (fitted to Eq. (3)) corresponding to H, H10T and H20T samples increase with the applied voltage and time. The driving

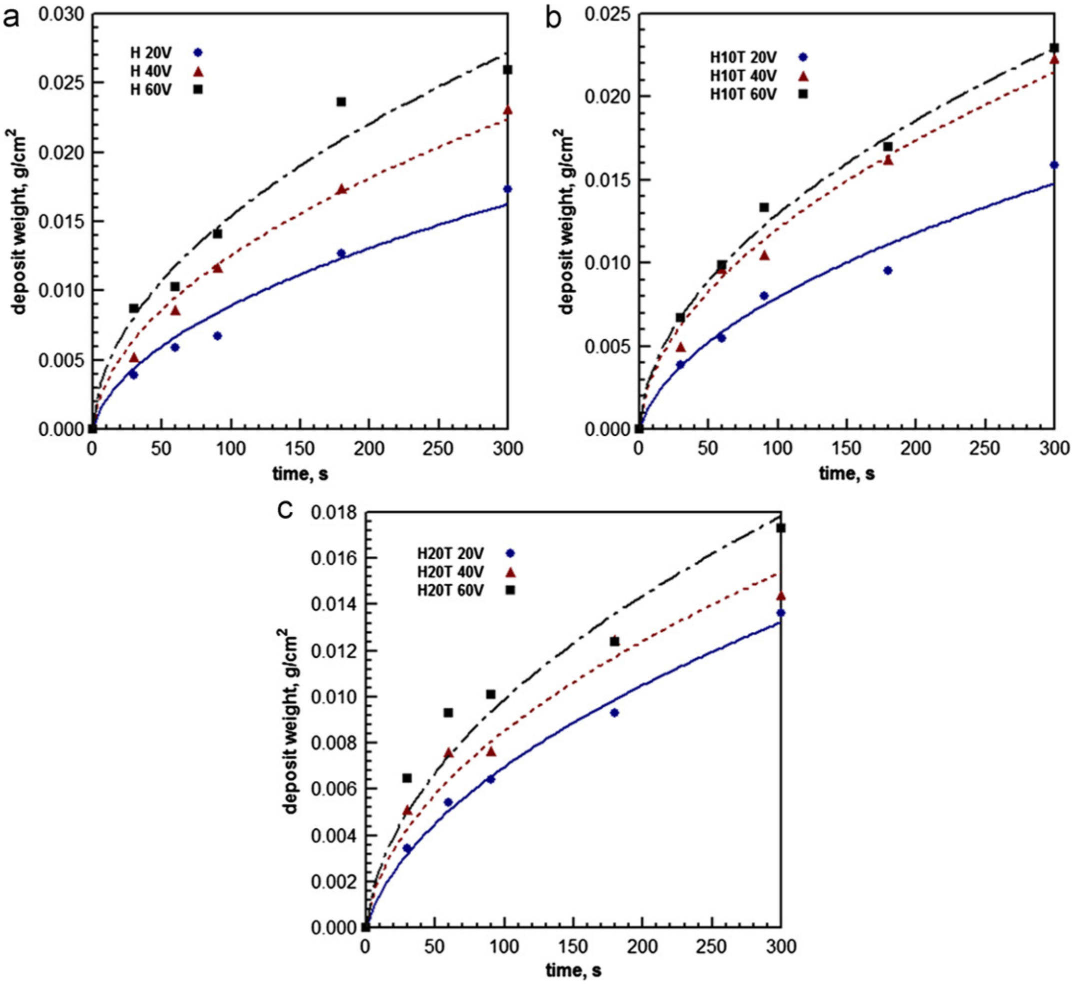

Fig. 8. Deposit weight of (a) H, (b) H10T, and (c) H20T samples as a function of deposition time (Eq. (3)) at different applied voltages.

force for electrophoretic deposition enhances by an increase in applied voltage; this results in a stronger columbic force acting on the charged suspended particles [23]. At moderate applied electrical fields (20–60 V/cm), the uniformity of deposited layers is more favorable, while the deposited layers may be disturbed by turbulence flows in the surrounding medium during the deposition at higher electrical fields [32]. On the other hand, the deposition rate decreases by increasing time and wt.% of TiO_2 (Fig. 9) because of a voltage drop across the deposited layer (shielding effect of growing layer [27,28,43]). The greater surface area of TiO_2 nanoparticles result in the higher electrolyte concentration and the lower zeta potential (Table 2). Thus, lower kinetic constants (α and k in Table 3) are expected in the case of HA–TiO_2 suspensions; i.e. the deposition yield decreases by the addition of TiO_2 nanoparticles to HA suspensions (Table 3). Fig. 10 shows the values of α and k constants in Eqs. (2–4) versus the applied voltage and wt% TiO_2. Again, the reduction in deposition rate due to TiO_2 addition is much more evident at higher deposition voltages where diffusion is the rate-determining step [50].

3.3. Development of RSM and effect of parameters

In order to shed more light on the effect of pertinent factors in the EPD system, response surface methodology is employed for the identification and quantification of the important parameters; the methodology which is able to simultaneously consider several parameters at different levels, and to give a suitable model for the relationship between the various factors and the response. Based on the results obtained in previous sections, the effects of voltage (V), time and wt% TiO_2 on deposit weight (W) are assessed. Table 1 lists the values of W at each of the 17 combination of factor levels generated by the principles of RSM. The results of the ANOVA are presented in Table 4; the low p values for the regression ($P < 0.01$) and the fact that the lack of fit of the model was not significant ($P > 0.05$) indicates the suitability of the model.

The values of the regression coefficients are presented in Table 5. Regarding the statistical criterion ($P < 0.05$), the linear and interactive terms of V and time are statistically significant at the initial times of deposition; however, all the linear terms of the factors are significant in the case of final

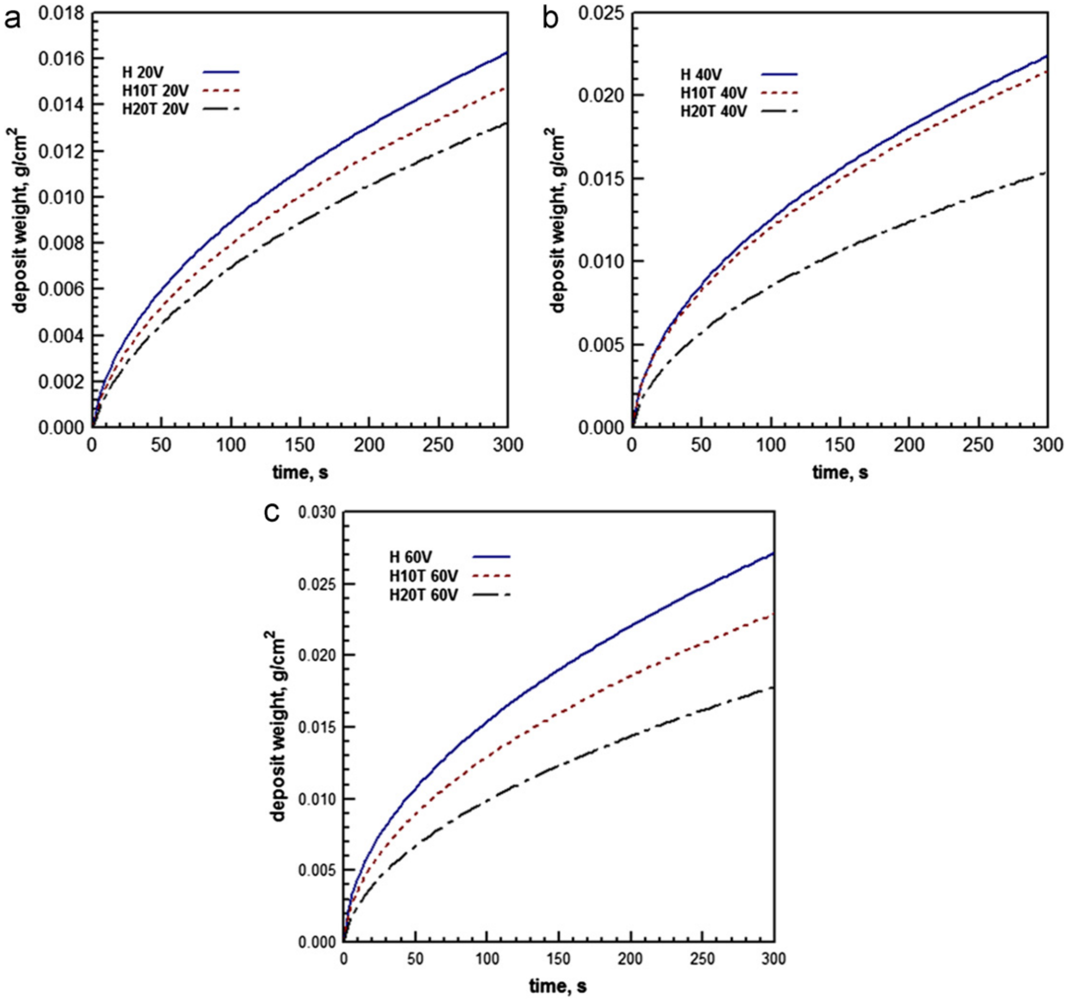

Fig. 9. Deposit weight as a function of deposition time (Eq. (3)) at different applied voltages: (a) 20 V, (b) 40 V, and (c) 60 V.

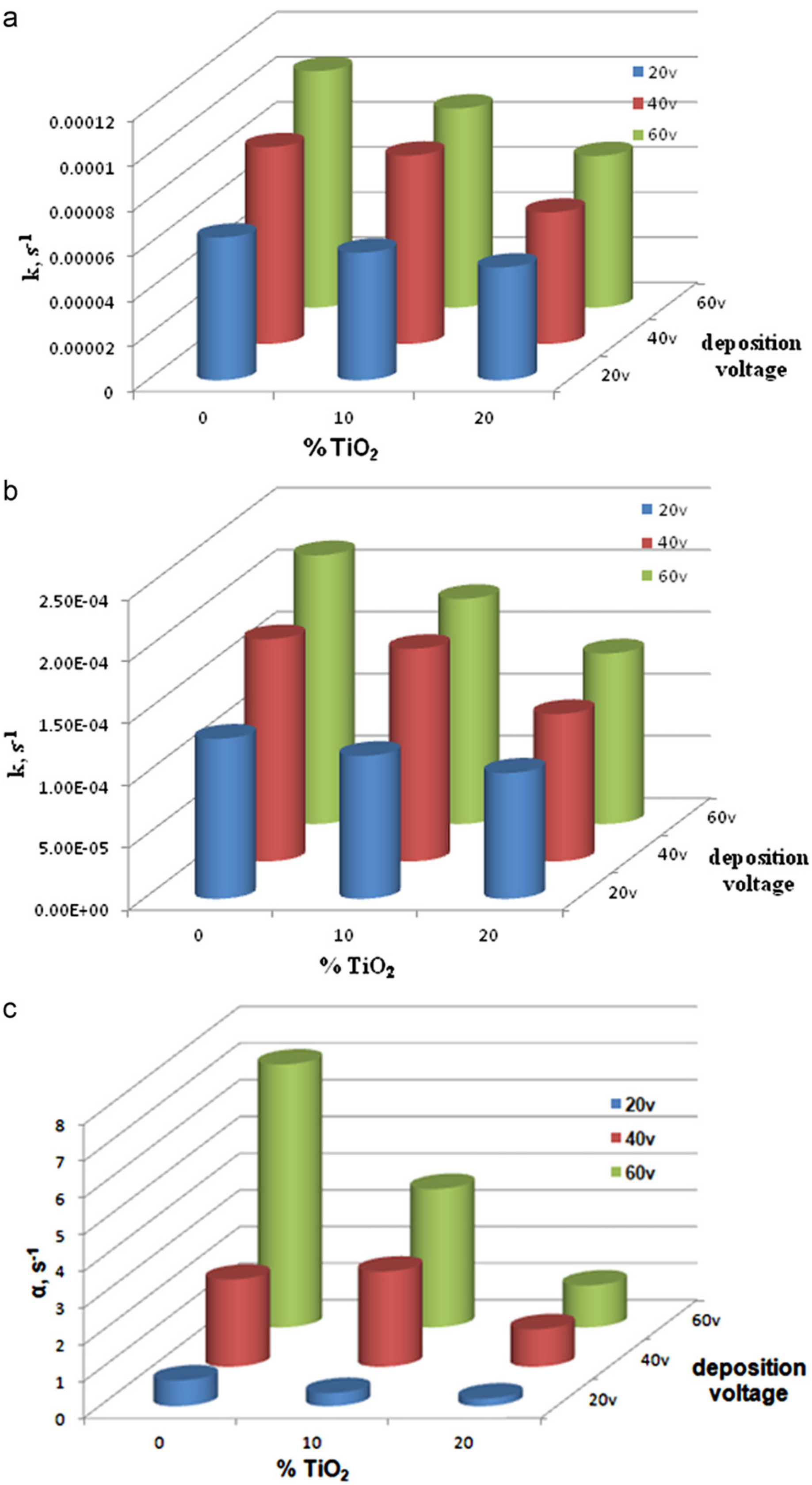

Fig. 10. Variation of kinetic constants obtained from (a) Eq. (1), (b) Eq. (2) and (c) Eq. (3) indicating deposition rate decreases by an increase in %TiO_2.

times of deposition (Table 5). Furthermore, the quadratic terms of V, time and $\%TiO_2$ as well as the interactive terms of time and $\%TiO_2$ shows significant statistical effect on W within 60–300 s. Accordingly, polynomial regression equations are proposed for the short and long deposition time periods:

$$10 < \text{time(s)} < 60 \tag{5}$$

$$W = 0.00514 + 0.00139V + 0.00311\ \text{time} + 0.0008V \times \text{time}$$

$$10 < \text{time(s)} < 300 \tag{6}$$

$$W = 0.016 + 0.0029V + 0.0057\ \text{time} - 0.00148\%TiO_2 - 0.00312V^2 - 0.00126\ \text{time} \times \%TiO_2$$

At short time interval, Eq. (5) can successfully predict the increasing trend of deposit weight by the both linear and interactive terms of V and time. Since $\%TiO_2$ term is insignificant in Eq. (5), TiO_2 particles have negligible contribution in deposition yield. It was reported that the initially deposited layers have a low solid fraction (3–5%) and a great porosity ($>95\%$) [51]. Therefore, at the initial times of deposition the rate of deposition is similar for all samples.

At long times of deposition, W increases with both V and time (Eq. (6)); however, the linear term of $\% TiO_2$, the quadratic term of V, and the interactive term of time and $\%TiO_2$ result in a decrease in W (negative sign of the coefficients) which implies the contribution of insulating layer [27,50].

In the cases where interaction between factors is statistically significant, contour plots give more complete information regarding the effect of a factor on the response. Fig. 11 shows the deposit weight map of H, H10T and H20T suspensions in the range of 60–300 s. As is clearly observed in Fig. 11a and b, at initial times (<100 s) and 20 V the deposit weight varies smoothly with $\%TiO_2$. During this period, both large and small particles are deposited because of their proximity to the cathode. At higher voltages (>20 V) and/or longer times (>100 s), the deposit yield mostly depends on $\%TiO_2$.

Fig. 12 illustrates the bilateral effects of time and $\%TiO_2$ on the deposit weight at long times of deposition (60–300 s) for different applied voltages. At voltage range of range 40–60 V, the electrical field is sufficiently strong to interact with the suspended particles, and consequently, the surface plots corresponding to 40 and 60 V are approximately similar. The reduction in deposit yield at high applied voltages (the negative sign of V^2 coefficient in Eq. (6)) originates from the insulating particles deposited on the electrode, which decreases the electrical field strength and driving force for further deposition [28,50]. In addition, the partial derivatives of Eqs. (5) and (6) with respect to time can be

Table 4
ANOVA table for W as the response in the short and long periods of deposition.

	W (10–60 s)					W (60–300 s)				
	df	SS	MS	*f*-Values	*p*-Values	df	SS	MS	*f*-Values	*p*-Values
Total	16	0.000126				16	0.000489			
Regression	9	0.000483	0.000014	75.06	0.000	9	0.000483	0.000054	62.54	0.000
Residual error	7	0.000001	0.000000			7	0.000006	0.000001		
Lack of fit (model error)	5	0.000001	0.000000	10.66	0.090	5	0.000006	0.000001	6.95	0.130
Pure error (Replicate error)	2	0.000000	0.000000			2	0.0000001	0.0000001		
R^2	91.88					97.19				

Abbreviations: *df*=degrees of freedom; SS=sum of squares; MS=mean squares.

Table 5
Values of regression coefficients calculated for the weight of deposition during EPD process (values are coded).

Independent factor	W (10–60 s)				W (60–300 s)			
	Regression coefficient	Standard error	*t*-Value	*p*-Value	Regression coefficient	Standard error	*t*-Value	*p*-Value
Constant	0.0057	0.00018	30.923	0.000	0.0164	0.00040	41.31	0.000
Linear								
V	0.0014	0.00014	10.230	0.000	0.0029	0.00030	9.833	0.000
time	0.0031	0.00014	22.906	0.000	0.0056	0.00030	19.290	0.000
$\%TiO_2$	−0.00024	0.00014	−1.746	0.124	−0.0015	0.00029	−5.053	0.001
Quadratic								
$V \times V$	0.00005	0.00026	0.202	0.846	−0.0031	0.0006	−5.431	0.001
time × time	−0.00039	0.00026	−1.494	0.179	−0.00032	0.0006	−0.571	0.586
$\%TiO_2 \times \%TiO_2$	−0.0006	0.00026	−2.200	0.064	0.00023	0.0006	0.401	0.701
Interactive								
$V \times$ time	0.00077	0.00015	5.106	0.001	0.0006	0.00033	1.794	0.116
$V \times \%TiO_2$	−0.00013	0.00015	−0.873	0.412	−0.0006	0.00033	−1.794	0.116
time × $\%TiO_2$	−0.00017	0.00015	−1.153	0.287	−0.0013	0.00033	−3.855	0.006

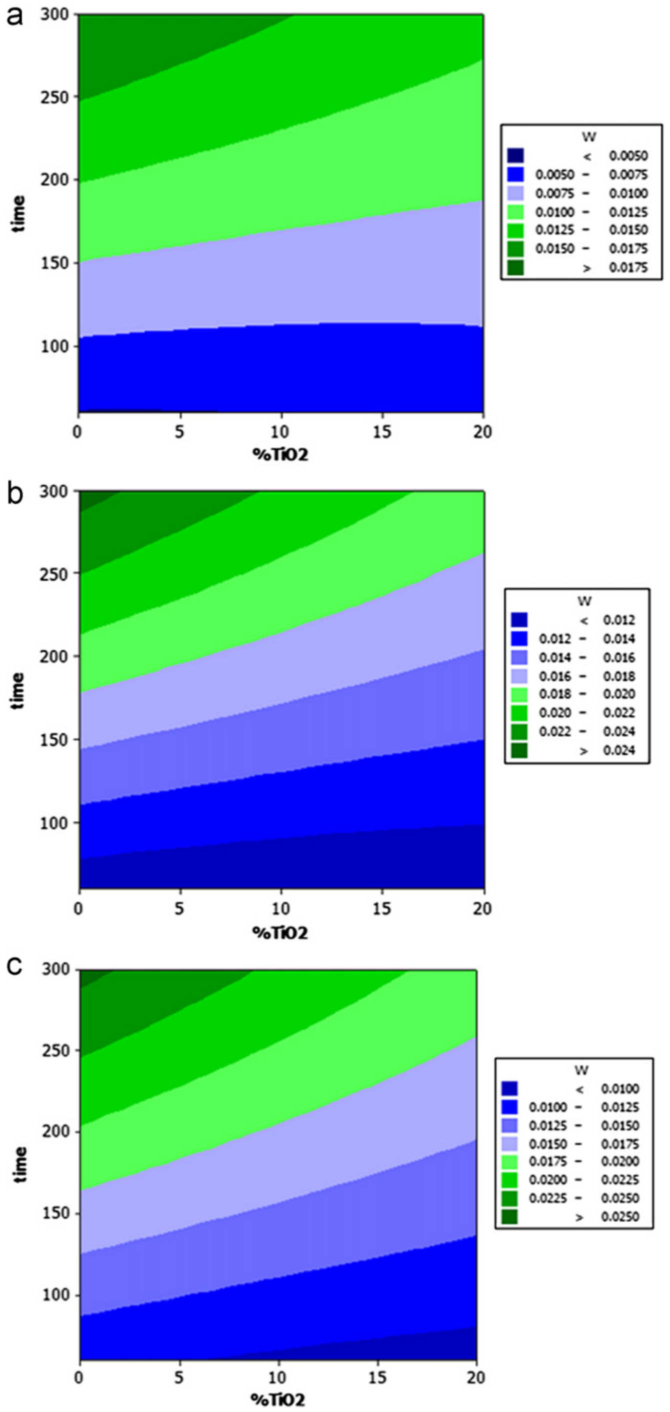

Fig. 11. Deposition yield map of (a) H, (b) H10T, and (c) H20T samples in the long period.

obtained as

$$\frac{\partial W}{\partial t} = 0.00311 + 0.0008V \quad 10 < time(\mathrm{s}) < 60 \tag{7}$$

$$\frac{\partial W}{\partial t} = 0.0057 - 0.00126\,\%\mathrm{TiO}_2 \quad 60 < time(s) < 300 \tag{8}$$

These two relations elucidate that the deposition rate is only V-dependent at short times (Eq. (7)) and at long times, the deposition rate drastically decreases by an increase in $\%\mathrm{TiO}_2$ (Eq. (8)).

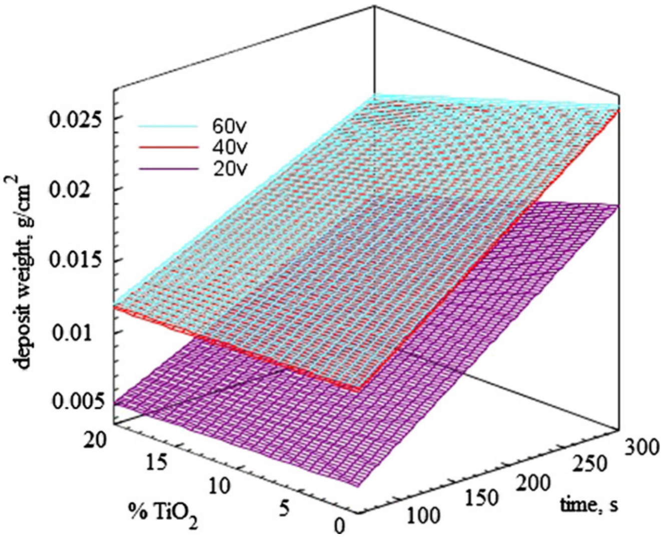

Fig. 12. Surface plots of deposition yield against time and $\%\mathrm{TiO}_2$ at different electric fields.

In order to verify the rate-controlling mechanism during EPD, Eqs. (1) and (2) are employed for short and long times of deposition (Fig. 13), respectively. In the case of $\alpha t \ll 1$ (red colored line in Fig. 13), Eq. (5) can be simplified to Hamaker equation as expected. At initial times, this can be explained in terms of the pressure exerted on initially deposited particles by those deposited later; van der Waals and steric forces overcome the electrostatic repulsion forces due to the particles compressing (deposition rate-controlling mechanism) [50]. However, at longer times (blue colored line in Fig. 13) the variation of deposit weight obeys Baldisserri equation. The progressive decrease in electrical conductivity of the deposit by increasing deposit thickness leads to a sharp reduction in electrical field at the outer deposit layer and accordingly, the driving force for further deposition decreases (diffusion controlled mechanism) [50]. Table 6 lists the regression constants corresponding to the best fitted equations with the experimental data in both linear and parabolic modes. The rate constants of H, H10T, and H20T samples are approximately similar in the linear mode which confirms the insignificancy of $\%\mathrm{TiO}_2$ term in Eqs. (5) and (7). Contrarily, at long times of deposition (parabolic regime, Eq. (8)) the value of α decreases with $\%\mathrm{TiO}_2$. According to Fig. 13, the critical time at transition mode is a function of $\%\mathrm{TiO}_2$ which subsequently decreases from 60 s (for H) to less than 20 s (for H20T). Additionally, a better particle packed structure can be achieved at shorter deposition times for H20T suspension. In linear mode, the pores are much less uniform both in size and distribution compared to those in parabolic mode. Nevertheless, the pores become much finer and more uniformly distributed by increasing $\%\mathrm{TiO}_2$.

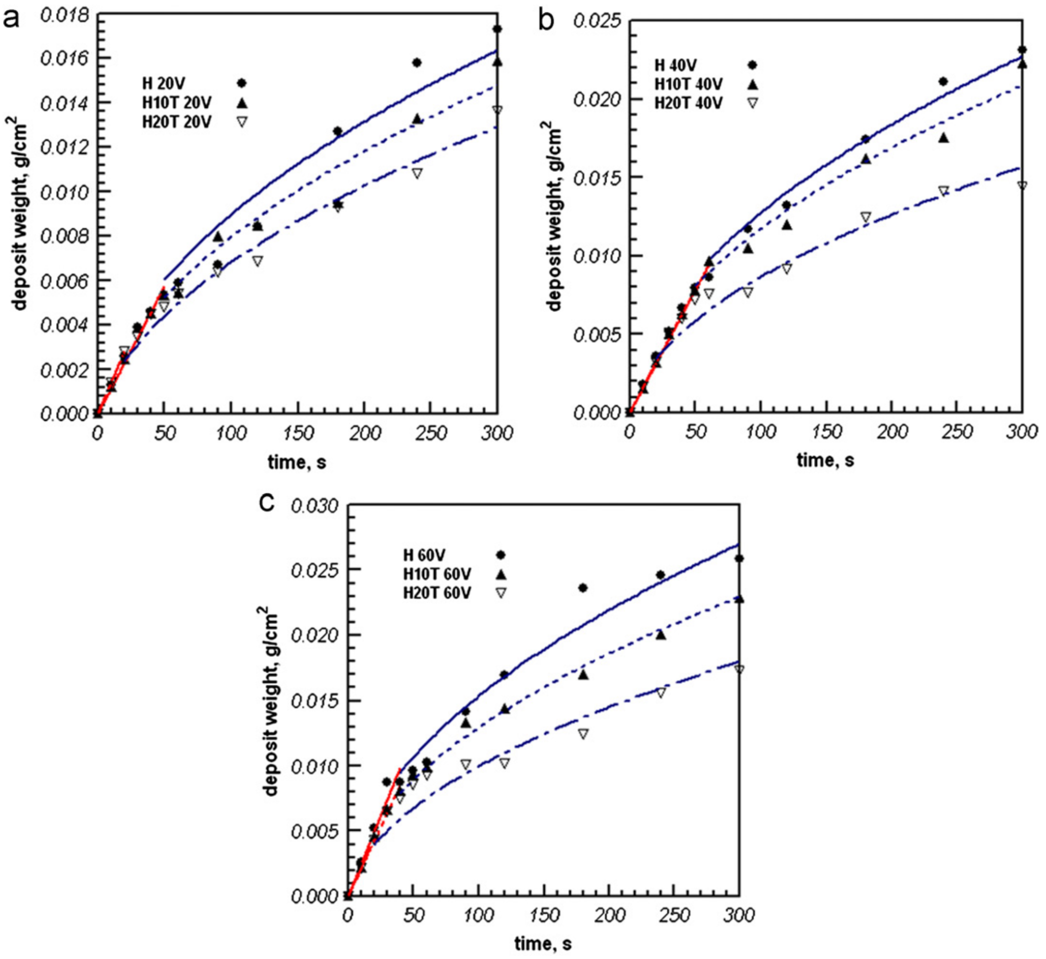

Fig. 13. Linear and parabolic deposition weight–time approach for short and long time periods of deposition at (a) 20 V, (b) 40 V, and (c) 60 V.

Table 6
Fitting constants obtained from Eqs. (1) and (3) in linear and parabolic modes.

Sample	Voltage (V)	Linear mode			Parabolic mode		
		$k \times 10^{-4}$ (s^{-1})	R^2	$\partial W/\partial t \times 10^{-4}$ (Eq. (7))	α (s^{-1})	R^2	$\partial W/\partial t \times 10^{-5}$ (Eq. (8))
H	20	1.15	0.9772	0.934	0.695	0.9368	5.76
	40	1.57	0.9788	1.24	2.31	0.9814	5.76
	60	2.47	0.9463	1.55	7.25	0.9621	5.76
H10T	20	1.14	0.9818	0.934	0.359	0.9505	4.71
	40	1.59	0.9985	1.24	2.75	0.9688	4.71
	60	2.13	0.9910	1.55	3.77	0.9910	4.71
H20T	20	1.39	0.9990	0.934	0.219	0.9766	3.66
	40	1.62	0.9990	1.24	0.987	0.9501	3.66
	60	2.16	0.9990	1.55	1.12	0.9010	3.66

4. Conclusions

The kinetics of electrophoretic deposition from HA–TiO_2 suspensions with 0, 10, and 20 wt% TiO_2 was investigated. Zeta potential and particle size distribution of the particles in suspensions were analyzed. The results reveal that an increase in the amount of TiO_2 nanoparticles in HA–TiO_2 suspension leads to a decrease in Zeta potential. According to SEM and AFM studies, the larger pores and higher surface roughness were observed in HA coatings, while the deposit layer was densified with increasing TiO_2 content in H10T, and H20T samples. Based on the deposition yields of HA–TiO_2 coatings under different voltages after 300 s, it was found that the conventional semi-empirical equations are not capable to predict precisely the rate of deposition. However, the new parabolic model proposed by Baldisserri that considers the shielding effect of growing layer can well reproduce the experimental data. This effect is responsible for the voltage drop across the deposited layer. A RSM-CCD was employed both at short (10–60 s) and long (60–300 s) time intervals of deposition to identify the relation/interrelation between parameters (i.e. voltage, time and %TiO_2) with the following results:

- The deposition yields corresponding to H, H10T and H20T suspensions increase with both applied voltage and time. However, the deposition rate decreases by an increase in wt% TiO_2 and time.
- The linear and interactive terms of voltage and time are significant at short times of deposition (10–60 s). However, %TiO_2 term is statistically insignificant which reveals that the deposition rate of H, H10T, and H20T samples is identical within 10–60 s of deposition.
- At longer times of deposition (60–300 s), deposition yield increases with applied voltage and time. However, the linear term of %TiO_2, the quadratic term of voltage, and the interactive term of time and %TiO_2 result in a decrease in deposition yield which implies the contribution of insulating deposit.
- After initial times of deposition, there is a transition from the linear mode to the parabolic mode. The critical transition time is a function of %TiO_2 and it decreases from 60 s (for H) to less than 20 s (for H20T).

References

[1] S.R. Paital, N.B. Dahotre, Calcium phosphate coatings for bio-implant applications: materials, performance factors, and methodologies, Materials Science and Engineering R 66 (2009) 1–70.

[2] C. Kailasanathan, N. Selvakumar, V. Naidu, Structure and properties of titania reinforced nano-hydroxyapatite/gelatin bio-composites for bone graft materials, Ceramics International 38 (2012) 571–579.

[3] T. Goto, I.Y. Kim, K. Kikuta, C. Ohtsuki, Hydroxyapatite formation by solvothermal treatment of α-tricalcium phosphate with water–ethanol solution, Ceramics International 38 (2012) 1003–1010.

[4] S. Murakami, K. Kato, Y. Enari, M. Kamitakahara, N. Watanabe, K. Ioku, Hydrothermal synthesis of porous hydroxyapatite ceramics composed of rod-shaped particles and evaluation of their fracture behavior, Ceramics International 38 (2012) 1649–1654.

[5] K. Venkateswarlu, N. Rameshbabu, A. Chandra Bose, V. Muthupandi, S. Subramanian, D. Mubarak Ali, N. Thajuddin, Fabrication of corrosion resistant, bioactive and antibacterial silver substituted hydroxyapatite/titania composite coating on Cp Ti, Ceramics International 38 (2012) 731–740.

[6] S. Sathish, M. Geetha, S.T. Aruna, N. Balaji, K.S. Rajam, R. Asokamani, Studies on plasma sprayed bi-layered ceramic coating on bio-medical Ti–13Nb–13Zr alloy, Ceramics International 37 (2011) 1333–1339.

[7] A. Dey, S.K. Nandi, B. Kundu, C. Kumar, P. Mukherjee, S. Roy, A.K. Mukhopadhyay, M.K. Sinha, D. Basu, Evaluation of hydroxyapatite and β-tri calcium phosphate microplasma spray coated pin intra-medullary for bone repair in a rabbit model, Ceramics International 37 (2011) 1377–1391.

[8] I. Sopyan, S. Ramesh, N.A. Nawawi, A. Tampieri, S. Sprio, Effects of manganese doping on properties of sol–gel derived biphasic calcium phosphate ceramics, Ceramics International 37 (2011) 3703–3715.

[9] A. Yelten, S. Yilmaz, F.N. Oktar, Sol–gel derived alumina–hydroxyapatite–tricalcium phosphate porous composite powders, Ceramics International 38 (2012) 2659–2665.

[10] H. Li, Z. Guo, B. Xue, Y. Zhang, W. Huang, Collagen modulating crystallization of apatite in a biomimetic gel system, Ceramics International 37 (2011) 2305–2310.

[11] D. Wei, Y. Zhou, Preparation, biomimetic apatite induction and osteoblast proliferation test of TiO_2-based coatings containing P with a graded structure, Ceramics International 35 (2009) 2343–2350.

[12] T.R. Rautray, R. Narayanan, K.H. Kim, Ion implantation of titanium based biomaterials, Progress in Materials Science 56 (2011) 1137–1177.

[13] H. Farnoush, J. Aghazadeh Mohandesi, D. Haghshenas Fatmehsari, F. Moztarzadeh, Modification of electrophoretically deposited nano-hydroxyapatite coatings by wire brushing on Ti–6Al–4V substrates, Ceramics International 38 (2012) 4885–4893.

[14] C. Kaya, Electrophoretic deposition of carbon nanotube-reinforced hydroxyapatite bioactive layers on Ti–6Al–4V alloys for biomedical applications, Ceramics International 34 (2008) 1843–1847.

[15] S. Subramanian, D. Mubarak Ali, N. Thajuddin, Fabrication of corrosion resistant, bioactive and antibacterial silver substituted hydroxyapatite/titania composite coating on Cp Ti, Ceramics International 38 (2012) 731–740.

[16] A.R. Boccaccini, S. Keim, R. Ma, Y. Li, I. Zhitomirsky, Journal of the Royal Society Interface 7 (2010) S581–S613.

[17] O. Albayrak, O.E. Atwani, S. Altintas, Hydroxyapatite coating on titanium substrate by electrophoretic deposition method: effects of titanium dioxide inner layer on adhesion strength and hydroxyapatite decomposition, Surface and Coatings Technology 202 (2008) 2482–2487.

[18] M. Wei, A.J. Ruys, M.V. Swain, B.K. Milthorpe, C.C. Sorrell, Hydroxyapatite-coated metals: interfacial reactions during sintering, Journal of Materials Science: Materials 16 (2005) 101–106.

[19] P.C. Rath, L. Besra, B.P. Singh, S. Bhattacharjee, Titania/hydroxyapatite bi-layer coating on Ti metal by electrophoretic deposition: characterization and corrosion studies, Ceramics International 38 (2012) 3209–3216.

[20] L. Mohan, D. Durgalakshmi, M. Geetha, T.S.N. Sankara Narayanan, R. Asokamani, Electrophoretic deposition of nanocomposite ($HAp+TiO_2$) on titanium alloy for biomedical applications, Ceramics International 38 (2012) 3435–3443.

[21] Y. Bai, K.A. Kim, I.S. Park, S.J. Lee, T.S. Bae, M.H. Lee, In situ composite coating of titania–hydroxyapatite on titanium substrate by micro-arc oxidation coupled with electrophoretic deposition processing, Materials Science and Engineering: B 176 (2011) 1213–1221.

[22] D.Y. Kim, M. Kim, H.E. Kim, Y.H. Koh, H.W. Kim, J.H. Jang, Formation of hydroxyapatite within porous TiO_2 layer by micro-arc oxidation coupled with electrophoretic deposition, Acta Biomaterialia 5 (2009) 2196–2205.

[23] B. Ferrari, R. Moreno, EPD kinetics: a review, Journal of the European Ceramic Society 30 (2010) 1069–1078.

[24] S. Bonnas, H.J. Ritzhaupt-Kleissl, J. Haußelt, Fabrication of particle and composition gradients by systematic interaction of sedimentation and electrical field in electrophoretic deposition, Journal of the European Ceramic Society 30 (2010) 1177–1185.

[25] H.C. Hamaker, Formation of a deposit by electrophoresis, Transactions of the Faraday Society 35 (1940) 279–287.

[26] Z. Zhang, Y. Huang, Z. Jiang, Electrophoretic deposition forming of SiC–TZP composites in a nonaqueous sol media, Journal of the American Ceramic Society 77 (1994) 1946–1949.

[27] C. Baldisserri, D. Gardini, C. Galassi, An analysis of current transients during electrophoretic deposition (EPD) from colloidal TiO_2 suspensions, Journal of Colloid and Interface Science 347 (2010) 102–111.

[28] K.T. Lau, C.C. Sorrell, Electrophoretic mobilities of dissolved polyelectrolyte charging agent and suspended non-colloidal titanium during electrophoretic deposition, Materials Science and Engineering: B 176 (2011) 369–381.

[29] S. Radice, C.R. Bradbury, J. Michler, S. Mischler, Critical particle concentration in electrophoretic deposition, Journal of the European Ceramic Society 30 (2010) 1079–1088.

[30] M. Mishra, S. Bhattacharjee, L. Besra, H.S. Sharma, Effect of pH localization on microstructure evolution of deposits during aqueous electrophoretic deposition (EPD), Journal of the European Ceramic Society 30 (2010) 2467–2473.

[31] G. Mohanty, L. Besra, S. Bhattacharjee, B.P. Singh, Optimization of electrophoretic deposition of alumina onto steel substrates from its suspension in iso-propanol using statistical design of experiments, Materials Research Bulletin 43 (2008) 1814–1828.

[32] J. Chen, H. Fan, X. Chen, P. Fang, C. Yang, S. Qiu, Fabrication of pyrochlore-free PMN-PT thick films by electrophoretic deposition, Journal of Alloys and Compounds 471 (2009) L51–L53.

[33] H. Farnoush, D. Haghshenas Fatmehsari, J. Aghazadeh Mohandesi, H. Abdoli, Evaluation of strengthening behavior of Al–AlN nanostructured composite by the use of modified Heckel model and response surface methodology, Journal of Alloys and Compounds 517 (2012) 45–53.

[34] D.F. Haghshenas, B. Bonakdarpour, E. Keshavarz Alamdari, B. Nasernejad, Optimization of physicochemical parameters for bioleaching of sphalerite by Acidithiobacillus ferrooxidans using shaking bioreactors, Hydrometallurgy 111 (2012) 22–28.

[35] H. Farnoush, D. Haghshenas Fatmehsari, A. Ekrami, The effect of pre-straining at intermediate temperatures on the mechanical behavior of high-bainite dual phase (HBDP) steels, Materials Science and Engineering: A 543 (2012) 224–230.

[36] C. Compson, M. Liu, L. Besra, D. Earl, Modeling electrophoretic deposition on porous non-conducting substrates using statistical design of experiments, Journal of the American Ceramic Society 89 (2006) 2787–2795.

[37] F. Pishbin, A. Simchi, M.P. Ryan, A.R. Boccaccini, A study of the electrophoretic deposition of Bioglass suspensions using the Taguchi experimental design approach, Journal of the European Ceramic Society 30 (2010) 2963–2970.

[38] F. Pishbin, A. Simchi, M.P. Ryan, A.R. Boccaccini, Electrophoretic deposition of chitosan/45S5 Bioglass composite coatings for orthopaedic applications, Surface and Coatings Technology 205 (2011) 5260–5268.

[39] D.C. Montgomery, in: Design and Analysis of Experiments, 6th ed., John Wiley & Sons, New York, 2006.

[40] K. König, S. Novak, A.R. Boccaccini, S. Kobe, The effect of the particle size and the morphology of alumina powders on the processing of green bodies by electrophoretic deposition, Journal of Materials Processing Technology 210 (2010) 96–103.

[41] R.S. Hyam, K.M. Subhedar, S.H. Pawar, Suspension stability studies for the electrophoretic deposition of boron films, Colloids and Surfaces A 297 (2007) 172–178.

[42] A.G. Bhosale, R. Joshi, K.M. Subhedar, R. Mishra, S.H. Pawar, Acetone mediated electrophoretic deposition of nanocrystalline SDC on NiO-SDC ceramics, Journal of Alloys and Compounds 503 (2010) 266–271.

[43] H. Abdoli, M. Zarabian, P. Alizadeh, S.K. Sadrnezhaad, Fabrication of aluminum nitride coatings by electrophoretic deposition: effect of particle size on deposition and drying behavior, Ceramics International 37 (2011) 313–319.

[44] S. Jailani, G.V. Franks, T.W. Healy, ζ Potential of nanoparticle suspensions: effect of electrolyte concentration, particle size, and volume fraction, Journal of the American Ceramic Society 91 (2008) 1141–1147.

[45] C.Q. Ning, Y. Zhou, In vitro bioactivity of a biocomposite fabricated from HA and Ti powders by powder metallurgy method, Biomaterials 23 (2002) 2909–2915.

[46] A. Ahmad, G.H. Awan, S. Aziz, Synthesis and application of TiO_2 nanoparticles, Pakistan Engineering Congress, in: 70th Annual Session Proceedings, 2006, pp. 404–412.

[47] P.N. Kumta, C. Sfeir, D.H. Lee, D. Olton, D. Choi, Nanostructured calcium phosphates for biomedical applications: novel synthesis and characterization, Acta Biomaterialia 1 (2005) 65–83.

[48] S. Nath, R. Tripathi, B. Basu, Understanding phase stability, microstructure development and biocompatibility in calcium phosphate–titania composites, synthesized from hydroxyapatite and titanium powder mix, Materials Science and Engineering C 29 (2009) 97–107.

[49] I. Zhitomirsky, L. GalOr, Electrophoretic deposition of hydroxyapatite, Journal of Materials Science: Materials in Medicine 8 (1997) 213–219.

[50] S.J. Ciou, K.Z. Fung, K.W. Chiang, The mathematical expression for kinetics of electrophoretic deposition and the effects of applied voltage, Journal of Power Sources 172 (2007) 358–362.

[51] C.-Y. Chen, S.-Y. Chen, D.-M. Liu, Electrophoretic deposition forming of porous alumina membranes, Acta Materialia 47 (1999) 2717–2726.